

**Toward Optimal Metal–Organic Frameworks for Adsorption Chillers
Insights from the Scale-Up of MIL-101(Cr) and NH₂-MIL-125**

Graf, Stefan; Redder, Florian; Bau, Uwe; de Lange, Martijn; Kapteijn, Freek; Bardow, André

DOI

[10.1002/ente.201900617](https://doi.org/10.1002/ente.201900617)

Publication date

2019

Document Version

Final published version

Published in

Energy Technology

Citation (APA)

Graf, S., Redder, F., Bau, U., de Lange, M., Kapteijn, F., & Bardow, A. (2019). Toward Optimal Metal–Organic Frameworks for Adsorption Chillers: Insights from the Scale-Up of MIL-101(Cr) and NH₂-MIL-125. *Energy Technology*, 8(1), Article 1900617. <https://doi.org/10.1002/ente.201900617>

Important note

To cite this publication, please use the final published version (if applicable).
Please check the document version above.

Copyright

Other than for strictly personal use, it is not permitted to download, forward or distribute the text or part of it, without the consent of the author(s) and/or copyright holder(s), unless the work is under an open content license such as Creative Commons.

Takedown policy

Please contact us and provide details if you believe this document breaches copyrights.
We will remove access to the work immediately and investigate your claim.

Toward Optimal Metal–Organic Frameworks for Adsorption Chillers: Insights from the Scale-Up of MIL-101(Cr) and NH₂-MIL-125

Stefan Graf, Florian Redder, Uwe Bau, Martijn de Lange, Freek Kapteijn, and André Bardow*

The metal–organic frameworks (MOFs) MIL-101(Cr) and NH₂-MIL-125 offer high adsorption capacities and have therefore been suggested for sustainable energy conversion in adsorption chillers. Herein, these MOFs are benchmarked to commercial Siogel. The evaluation method combines small-scale experiments with dynamic modeling of full-scale adsorption chillers. For the common temperature set 10/30/80 °C, it is found that MIL-101(Cr) has the highest adsorption capacity, but considerably lower efficiency (–19%) and power density (–66%) than Siogel. NH₂-MIL-125 increases efficiency by 18% compared with Siogel, but reduces the practically important power density by 28%. From the results, guidelines for MOF development are derived: High efficiencies are achieved by matching the shape of the isotherms to the specific operating temperatures. By only adapting shape, efficiencies are 1.5 times higher. Also, higher power density requires matching the shape of the isotherms to create high driving forces for heat and mass transfer. Second, if MOFs' heat and mass transfer coefficients could reach the level of Siogel, their maximum power density would double. Thus, development of MOFs should go beyond adsorption capacity, and tune the structure to the application requirements. As a result, MOFs could to serve as optimal adsorbents for sustainable energy conversion.

1. Introduction

More than 20 000 different metal–organic frameworks (MOFs) have been studied in recent years.^[1] MOFs are highly crystalline and porous adsorbents with a high pore volume and surface area,^[2] made from metal-containing units connected by organic ligands. Both, the metal-containing units and the organic ligands, can be varied almost indefinitely, which allows tuning the MOF structure to specific applications,^[3] as demonstrated, e.g., for carbon capture,^[4–6] natural gas purification,^[7] storage of methane^[8–10] or hydrogen,^[11] and for electrochemical applications.^[12]

Recently, MOFs have also been shown to be highly efficient adsorbents for water.^[13] Efficient water adsorption enables natural gas dehydration,^[11] water harvesting from humid air,^[14,15] thermal energy storage,^[16] and sustainable thermal energy conversion, as discussed for adsorption heat pumps and adsorption chillers by de Lange et al.^[17] The application of MOFs in adsorption chillers seems highly promising to enable sustainable cooling, as water can be used as a natural and safe refrigerant and the driving energy is low-temperature heat, which is readily available from solar, geothermal, or waste sources. In adsorption chillers, MOFs adsorb water, which is evaporated to satisfy a cooling demand. For regeneration, the MOF is desorbed by low-temperature heat, making the adsorption chiller a sustainable alternative to conventional chillers.^[18,19]


Besides water as refrigerant, ethanol and methanol are investigated as refrigerants together with MOFs in adsorption chillers.^[20,21] The working pair MIL-101(Cr)/ethanol shows very high adsorption capacities up to 1.2 kg kg^{–1}.^[22] Kummer et al.^[23] investigated MIL-101(Cr) with methanol as refrigerant and found the uptake twice as high as for activated carbon. Yet, in this study, we focus on water as refrigerant since it has a global warming potential (GWP) of zero and is easily applicable.

The great potential of MOFs for adsorption chillers is due to the high adsorption capacity.^[24–26] For the most promising MOF MIL-101(Cr) with water as refrigerant, an analysis of the equilibrium properties suggests a high efficiency in terms of a high coefficient of performance (COP) of 0.89, which is 29% higher

Dr. S. Graf, F. Redder, Dr. U. Bau, Prof. A. Bardow
Institute of Technical Thermodynamics
RWTH Aachen University
Schinkelstraße 8, 52062 Aachen, Germany
E-mail: andre.bardow@ltt.rwth-aachen.de

Dr. M. de Lange, Prof. F. Kapteijn
Catalysis Engineering
Delft University of Technology
Van der Maasweg 9, 2629 HZ Delft, The Netherlands

Prof. A. Bardow
Institute of Energy and Climate Research, Energy Systems Engineering (IEK-10)
Forschungszentrum Jülich GmbH
Wilhelm-Johnen-Straße, 52425 Jülich, Germany

 The ORCID identification number(s) for the author(s) of this article can be found under <https://doi.org/10.1002/ente.201900617>.

© 2019 The Authors. Published by WILEY-VCH Verlag GmbH & Co. KGaA, Weinheim. This is an open access article under the terms of the Creative Commons Attribution-NonCommercial License, which permits use, distribution and reproduction in any medium, provided the original work is properly cited and is not used for commercial purposes.

DOI: 10.1002/ente.201900617

compared with the commercial benchmark AQSOA-Z02.^[17] The high efficiency is very promising, but this estimate only considered the MOF's isotherms. The actual performance in an adsorption chiller is more complex: The performance strongly depends on heat transfer and diffusion resistances in the actual configuration of the full-scale adsorption chiller.^[27] Low heat transfer and diffusion coefficients lead to low power density, a major drawback of adsorption chillers.^[28] Thus, an analysis of the actual potential of MOFs for adsorption chillers requires both efficiency and power density for a full-scale adsorption chiller.^[29,30]

For power density, a heuristic specific cooling power (SCP) was determined for the MOFs NH₂-MIL-125 and MOF-801 with water, suggesting a high power density compared with benchmark materials.^[25,31] Lenzen et al.^[32] recently also determined the power density from a heuristic for the MOF CAU-10-H. The power density was in the same range as for benchmark materials. Progress is hampered by the fact that performance assessments require large amounts of MOF. For example, Lenzen et al.^[32] required 157 g of the MOF CAU-10-H to determine the power density in a full-scale adsorption chiller.

However, MOFs are more complex to synthesize compared with, e.g., zeolites and therefore are still much more expensive.^[6] First MOFs can already be synthesized under rather mild conditions (ambient temperature and water as the sole solvent) and thus more cost efficient. Also, continuous flow and extrusion synthesis allow to synthesize MOFs at a larger scale.^[33] Yet, their applicability for adsorption chiller applications needs to be proven.^[32,34,35] Thus, often, only small amounts of MOF samples are available, especially at the early development of new MOFs, being insufficient for evaluation in a full-scale adsorption chiller. Hence, we investigate MOFs for use in adsorption chillers by small-scale experiments, which still allows us to parametrize a full-scale adsorption chiller model.

For this purpose, we characterize MOFs in infrared-large-temperature-jump (IR-LTJ) experiments to extract heat transfer and diffusion coefficients.^[36] We combine the IR-LTJ method with dynamic modeling and optimization of a full-scale adsorption chiller to determine the efficiency and power density.^[37] The full-scale model allows examining the performance, without the need for a complete adsorption chiller setup.

We investigate the promising MOFs MIL-101(Cr) and NH₂-MIL-125 with the refrigerant water. MIL-101(Cr) was first synthesized by Férey et al.^[38] and the water sorption isotherms were first described by Khutia et al.^[39] We choose MIL-101(Cr), since it has the highest reported maximum adsorption capacity with 1.7 g g⁻¹, leading to an estimated COP efficiency (for a cooling application) of 0.89, as mentioned earlier. The water isotherms of NH₂-MIL-125 were first described by Jeremias et al.^[40] The maximum adsorption capacity of NH₂-MIL-125 is with 0.45 g g⁻¹ in the same range as for silica gels; however, in an adsorption chiller process, the maximum adsorption capacity is limited by the process temperatures.^[41] For typical temperatures in an adsorption chiller process (temperature set 10/30/80 °C^[42,43]), NH₂-MIL-125's adsorption capacity is still 0.38 g g⁻¹, while for silica gel (Fuji RD) it decreases to 0.11 g g⁻¹.^[31] Besides the high adsorption capacity of MIL-101(Cr) and NH₂-MIL-125, both MOFs have been shown to be water stable either for multiple cycles or direct immersion in boiling water for 1 week.^[17,44]

Kim et al.^[45] found MIL-101(Cr) to be stable for 10 cycles. Furthermore, certain MOFs have shown to be stable for thousands of cycles without performance losses.^[3] In addition to NH₂-MIL-125 and MIL-101(Cr), we also investigate the silica gel Siogel^[46] as a broadly discussed benchmark for adsorption chillers.

We find that only NH₂-MIL-125 reaches efficiencies higher than the commercially available adsorbent Siogel but at considerably lower power densities. MIL-101(Cr) has the highest adsorption capacity. Still, it has both considerably lower efficiencies and power densities than Siogel. These findings show that maximizing adsorption capacity can be a misleading design criterion for MOFs. To guide future MOF design, we show how the equilibrium properties have to match the application. Current MOFs have poorly positioned isotherms, reducing the efficiency and power density. In addition, low heat transfer and diffusion coefficients reduce power density. From our findings, we derive properties of an optimal MOF and develop novel design guidelines for MOFs to increase the performance in thermal energy conversion applications.

In Section 2, we briefly present the methods to describe the equilibrium properties, to determine the heat and mass transfer coefficients, and to determine the efficiency and power density of the investigated materials. In Section 3, we present the resulting efficiency and power density of the investigated materials and discuss how to increase the performance of MOFs compared with the commercially available adsorbent Siogel. Finally, we conclude the study in Section 4.

2. Model-Based Scale-Up of Small-Scale Experiments

In this section, we combine small-scale experiments with full-scale modeling to investigate MOFs for full-scale adsorption chillers. For this purpose, we briefly introduce the Dubinin model describing the equilibrium properties of the investigated materials (see Section 2.1). In Section 2.2, we summarize the small-scale experiment, the so-called IR-LTJ method, to extract heat transfer and diffusion coefficients. We use heat transfer and diffusion coefficients in a dynamic model of a complete adsorption chiller to determine the efficiency and power density in terms of the COP and volumetric cooling power (VCP), respectively. The adsorption chiller model is described in Section 2.3.

2.1. Describing the Equilibrium Characteristics

To describe the adsorption equilibrium, the loading of the adsorbent w as a function of temperature T and pressure p , we use the Dubinin model.^[47] In the Dubinin model, the loading w is modeled via the filled pore volume W

$$W(A) = \frac{w}{\rho_l(T_{ad})} \quad (1)$$

with $\rho_l(T_{ad})$ as the liquid density of water at adsorbent temperature T_{ad} . Essential for Dubinin's theory is that the filled pore volume W is a function of the adsorption potential A ,

which itself is a function of adsorbent temperature T_{ad} and pressure p_{ad}

$$A = RT_{ad} \ln \left(\frac{p_{sat}(T_{ad})}{p_{ad}} \right) \quad (2)$$

with the universal gas constant R and saturation pressure of water vapor at given temperature $p_{sat}(T_{ad})$.

The function of the pore volume $W(A)$ is called characteristic curve, see **Figure 1**. To describe the characteristic curve $W(A)$, we use the arctangent function,^[48] which describes the equilibrium properties of various working pairs.

$$W(A) = \frac{-\Delta W}{\pi} \arctan \left(\frac{A - A_{infl}}{A_{slope}} \right) + \left(W_0 - \frac{\Delta W}{2} \right) \quad (3)$$

The arctangent function directly allows interpreting the characteristic curve's parameters: The parameter ΔW describes the theoretical, maximum change in pore volume, which is equivalent to the maximum change in loading (cf. Equation (1)); the parameter W_0 describes the maximum (absolute) pore volume; the parameter A_{slope} describes the slope of the function, for small values, e.g., for $A_{slope} = 1 \text{ kJ kg}^{-1}$, the function's shape becomes step like; and the parameter A_{infl} sets the inflection point of the function.

The adsorbent materials were synthesized at TU Delft, following synthesis routes from the literature.^[49] Furthermore, the adsorbent materials were filtered and washed with hot water and dried at 160°C in air to remove any solvents. In our laboratories, the adsorbent materials did not come in direct contact with any solvents.

The investigated adsorbents were synthesized manually under laboratory conditions. Therefore, the equilibrium properties can differ for each synthesis and the literature data might not accurately describe the equilibrium properties of the present adsorbents $\text{NH}_2\text{-MIL-125}$ and MIL-101(Cr) . Thus, we redetermined the equilibrium properties of the adsorbents. For details of the measurement procedure and experimental results, see Section B,

Supporting Information. The determined equilibrium properties agree well with the values from literature.^[49]

2.2. Determining Heat and Mass Transfer Coefficients with the IR-LTJ Method

To determine the performance of MOFs in adsorption chillers, not only are equilibrium properties necessary, but also effective heat transfer and diffusion coefficients U_{eff} and D_{eff} . To determine the effective heat transfer and diffusion coefficients U_{eff} and D_{eff} , we use the IR-LTJ experiment with dynamic modeling.^[36] For an IR-LTJ experiment, only a small sample of adsorbent material of less than 250 mg is necessary, allowing to assess MOFs at an early stage of material development.

In an IR-LTJ experiment, we place the adsorbent in a packed-bed configuration with a bed height of 1 mm. We impose a temperature jump on the adsorbent, leading to adsorbing water vapor from a constant vapor volume. In the constant vapor volume, the pressure decreases. The temperatures of the adsorbent and of the sample carrier are recorded. The pressure and temperature information is used in a dynamic model, consisting of energy and mass balances of the adsorbent and the vapor phase, as well as equations for heat and mass transfer. We invert the model to determine time-resolved values of the heat transfer coefficient U_{eff} and the mass transfer coefficient D_{eff} . The values are time averaged for further use in the model of the adsorption chiller. Further information on the experimental setup and the dynamic model can be found in Section C Supporting Information, and in studies by Graf et al.^[36]

In this study, we determine effective heat transfer and diffusion coefficients for a reference case of a cooling application with an evaporation temperature of $T_{evap} = 10^\circ\text{C}$, a condensation and adsorption temperature of $T_{cond} = T_{ads} = 30^\circ\text{C}$, and a desorption temperature of $T_{des} = 80^\circ\text{C}$ ($10/30/80^\circ\text{C}$). This temperature set represents typical working conditions of an adsorption chiller for air-conditioning applications.^[42,43] In studies by Graf et al.,^[50] we showed that the such determined heat transfer and diffusion coefficients are also valid for other temperatures with high accuracy. Therefore, we use the same effective heat transfer and diffusion coefficients for other temperature sets.

2.3. Determining the Performance of an Adsorption Chiller

The effective heat transfer and diffusion coefficients U_{eff} and D_{eff} are used in a dynamic model of a thermal energy conversion application. In this study, we investigate the performance of MOFs exemplarily for adsorption chillers. The adsorption chiller configuration consists of the adsorbent placed on a heat exchanger (together called the adsorber), an evaporator, and a condenser and is based on the adsorption chiller constructed by Lanzerath et al.^[51]

The MOFs are evaluated for a packed-bed configuration in a finned-tube heat exchanger (**Figure 2**). In packed-bed configurations, interparticle mass transport resistances are low; however, heat transport resistances are considered higher as, e.g., in consolidated layer configurations.^[28] To account for the higher heat transport resistances in a packed-bed configuration, we choose a bed height of 1 mm only in the adsorber (cf. Figure 2). The bed

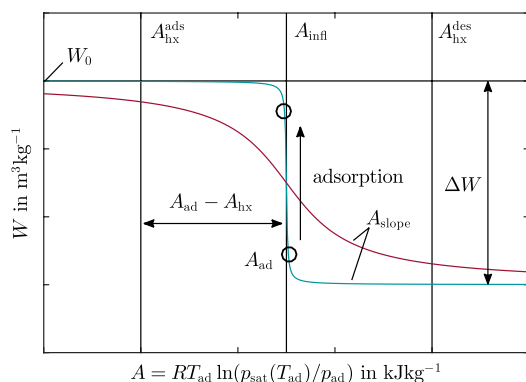


Figure 1. Schematic characteristic curve $W(A)$: pore volume W (cf. Equation (1)) as a function of the adsorption potential A (cf. Equation (2)). The characteristic curve is described by a trigonometric function (Equation (3)) with the following parameters: maximum change in pore volume ΔW , maximum pore volume W_0 , slope A_{slope} , and inflection point A_{infl} .

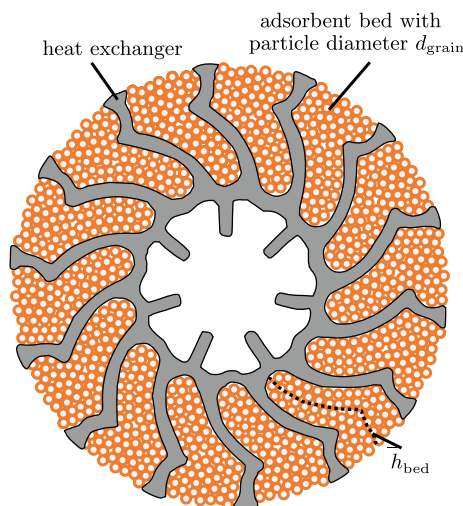


Figure 2. Adsorber structure: the heat exchanger is made from extruded aluminum pipes with fins. The adsorbent material is placed as a packed bed between the fins, as in studies by Lanzerath et al.^[51] Mean height of the adsorbent bed is $h_{\text{bed}} = 1$ mm. Geometric properties of the adsorber are shown in Table 1.

height is the same height as for the IR-LTJ experiments (cf. Section 2.2), allowing us to use the determined heat transfer and diffusion coefficients U_{eff} and D_{eff} in the adsorption chiller model. We use a finned-tube heat exchanger as a well-balanced compromise between high efficiency and power density;^[52] we use water as a refrigerant, since it is environmentally friendly and nontoxic compared to, e.g., ammonia or methanol. The geometry of the adsorber is based on the adsorption chiller constructed by Lanzerath et al.^[51]

In this study, we limit the volume of the adsorber for all investigated adsorbent materials to determine only the influence of the adsorbent material on efficiency and power density. For a limited volume, the density of the adsorbent ρ_{bed} has a strong influence on the overall performance of the system, as the mass of the adsorbent changes with bed density. As we restrict the adsorber volume, we use the VCP as a measure for power density. The parameters of the adsorber are summarized in Table 1.

The adsorber has already been modeled in a complete adsorption chiller in previous studies^[51] and has been experimentally validated using the working pair silica gel 123/water. The adsorber model showed excellent agreement between simulated and measured efficiency and power density. Thus, in this study,

Table 1. Parameters of adsorber geometry, as given in Lanzerath et al.^[51] Outer surface area A_{Ads} is the contact area of adsorber and adsorbent material.

Outer area	A_{Ads}	2.154 m ²
Adsorbent bed height	h_{sor}	1 mm
Adsorbent bed volume	V_{sor}	0.002154 m ³
Tube length	l_{Ads}	6.799 m
Mass	m_{Ads}	4.212 Kg
Specific heat capacity	c_{Ads}	0.888 kJ kg ⁻¹ K ⁻¹

we use the same adsorber model, consisting of models for the adsorbent, the heat exchanger, and mass transfer. The adsorber model is inserted in a full-scale adsorption chiller model, including the evaporator and the condenser (cf. Figure 3).

The models are based on the open-source adsorption systems library SorpLib,^[53] using the object-oriented modeling language Modelica.^[54] The adsorbent model describes the equilibrium properties of the working pair (cf. Section 2.1) and determines the energy released during adsorption or needed during desorption. The heat exchanger model includes the sensible heat of the heat exchanger geometry and the heat transfer between the adsorbent and heat exchanger with the determined heat transfer coefficient U_{eff} (cf. Section 2.2). To resolve only the performance of the adsorbent material, evaporator and condenser are modeled as ideal components, neglecting any pressure drops or heat losses. Thus, the calculated values for the efficiency and power density are an upper bound for the performance of the MOFs. The mass transfer models describe the mass transfer with the linear-driving-force approach^[55] and the determined diffusion coefficient D_{eff} (cf. Section 2.2). To model the fluid properties of water, we use the TILMedia library.^[56] TILMedia uses REFPROP^[57] with data from Cox et al.^[58] and Chase.^[59] Further details of the adsorption chiller model can be found in Section D, Supporting Information.

Inputs of the adsorption chiller model are the equilibrium properties, heat transfer and diffusion coefficients, and the process temperatures. In this work, we study a reference case with the temperature set 10/30/80 °C (cf. Section 2.2). To determine the effect of temperature on the MOFs' performance, we additionally investigate a condensation and adsorption temperature

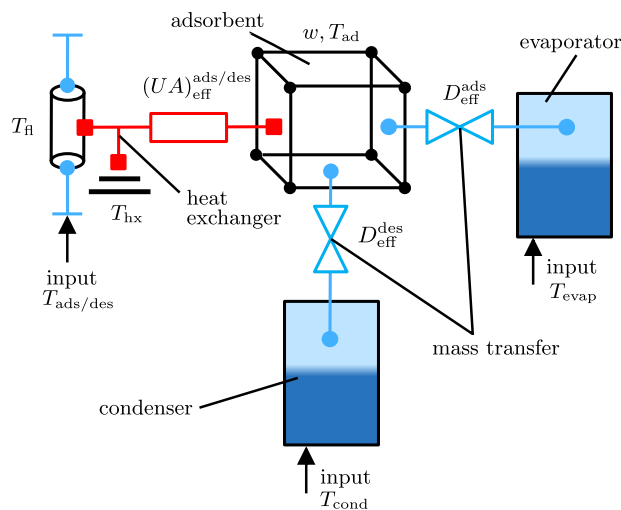


Figure 3. Scheme of the adsorption chiller model, consisting of models for adsorbent, heat and mass transfer, evaporator, and condenser. Inputs are the temperatures of the adsorber inlet during adsorption T_{ads} and desorption T_{des} , the temperature of the ideal condenser T_{cond} , the temperature of the ideal evaporator T_{evap} , and the times for adsorption and desorption τ_{ads} and τ_{des} . Differential states are temperature T_{ad} and loading w of adsorbent, temperatures of heat exchanger T_{hx} , and heat exchanger fluid T_{fl} . The effective heat transfer and diffusion coefficients U_{eff} and D_{eff} are determined with the IR-LTJ method (cf. Section 2.2). Outputs are efficiency and power density in terms of the COP and the VCP, respectively.

of 20 °C (resulting temperature set 10/20/80 °C) and a desorption temperature of 60 °C (10/30/60 °C).

The adsorption chiller model simulates heat flows and allows to determine the efficiency (COP) and the power density (VCP). The efficiency COP relates the provided cooling energy Q_{evap} to the needed energy to regenerate the adsorber Q_{reg}

$$\text{COP} = \frac{Q_{\text{evap}}}{Q_{\text{reg}}} = \frac{\int_0^{\tau_{\text{ads}}} \dot{Q}_{\text{evap}} dt}{\int_{\tau_{\text{ads}}}^{\tau_{\text{des}}} \dot{Q}_{\text{ads}} dt} \quad (4)$$

The power density VCP is a measure for the size of the adsorption chiller and relates the mean cooling power $Q_{\text{evap}}/(\tau_{\text{ads}} + \tau_{\text{des}})$ to the volume of the adsorber V_{ads}

$$\text{VCP} = \frac{Q_{\text{evap}}}{V_{\text{ads}} \cdot (\tau_{\text{ads}} + \tau_{\text{des}})} = \frac{\int_0^{\tau_{\text{ads}}} \dot{Q}_{\text{evap}} dt}{V_{\text{ads}} \cdot (\tau_{\text{ads}} + \tau_{\text{des}})} \quad (5)$$

Often, the mean cooling power is related to the adsorbent mass, leading to the SCP.^[29] The SCP is more important in applications where mass is restricted, e.g., in mobile applications. In contrast, the power density VCP assesses the size of the system: If the power density VCP is low, the volume of the adsorbent material is larger, leading to a larger heat exchanger and thus overall adsorber.

For a 1-bed adsorber, as in this study, the control strategy is determined from the times for adsorption τ_{ads} and desorption τ_{des} . The optimal times for adsorption and desorption are affected by the equilibrium properties and the heat transfer and diffusion coefficients. Thus, the optimal times for adsorption and desorption are specific for each adsorbent. A comparison of adsorbents is only consistent after determining optimal times for adsorption and desorption for each adsorbent.^[37] Otherwise, the comparison would mix adsorbent properties with the impact of suboptimal operation. Efficiency and power density represent two opposing objectives: Long times for adsorption and desorption increase the efficiency but decrease the power density and vice versa. This results in a multiobjective optimization problem with the objective functions efficiency and power density. We solve the optimization problem using the dynamic optimization algorithm MUSCOD II,^[60] resulting in a Pareto frontier regarding the efficiency and power density.

The presented model for the 1-bed adsorption chiller allows to predict the efficiency and power density with high accuracy when compared with full-scale experiments: For a 1-bed adsorber using silica gel, we found that both COP and the cooling power VCP are predicted within the measurement of the full-scale experiment. The predicted COP differed less than 7% and the cooling power

VCP less than 2% on average compared with full-scale experiments.^[61]

3. Performance and the Potential of MOFs in Adsorption Chillers

In this section, we present and discuss our findings for the investigated MOFs MIL-101(Cr) and NH₂-MIL-125 and the commercially available adsorbent Siogel: In Section 3.1, we present the equilibrium properties of the investigated materials. From the IR-LTJ experiments, we determine heat transfer and diffusion coefficients (Section 3.2). From the equilibrium properties and heat transfer and diffusion coefficients, we determine the efficiency and power density (Section 3.3). In Section 3.4, we discuss possible improvements of MOFs to increase the performance of adsorption chillers.

3.1. Equilibrium Characteristics

In this study, we investigate the MOFs MIL-101(Cr) and NH₂-MIL-125 and the commercial benchmark Siogel as reference, all with water as refrigerant. **Table 2** shows the adsorbent properties and **Figure 4** shows the characteristic curves of the investigated materials (for experimental data, see the ESI, Section B, Supporting Information). For a better interpretation, we multiplied the characteristic curve with the constant density of water $\rho_{\text{ad}} = 1000 \text{ kg m}^{-3}$ to receive the loading w (cf. Equation (1)) (right axis in Figure 4a,b). The MOF MIL-101(Cr) has the highest maximum loading (adsorption capacity), followed by NH₂-MIL-125 and Siogel.

However, the highest maximum loading is not achieved in an actual adsorption chiller cycle due to the corresponding temperature settings. For an adsorption chiller application, the reference temperature set is typically 10/30/80 °C (cf. Section 2.3). We transform these temperatures into adsorption potentials (Equation (2)). The adsorption potential at the end of adsorption $A_{\text{hx}}^{\text{ads}}(T_{\text{ads}}, p_{\text{evap}})$ is basically the difference of the vapor pressure of water at the adsorption temperature T_{ads} and the actual pressure provided by the evaporator at the temperature T_{evap} and measures the driving force for adsorption for an indefinite adsorption time. The corresponding pore volume $W(A_{\text{hx}}^{\text{ads}})$ is the maximum reachable pore volume for the given application. In analogy, we determine the adsorption potential at the end of desorption $A_{\text{hx}}^{\text{des}}(T_{\text{des}}, p_{\text{cond}})$ and the corresponding pore volume $W(A_{\text{hx}}^{\text{des}})$. The change in pore volume $W(A_{\text{hx}}^{\text{ads}}) - W(A_{\text{hx}}^{\text{des}})$ can be

Table 2. Equilibrium properties, heat capacity c_p , grain size d_{grain} , and bed density ρ_{bed} of investigated materials MIL-101(Cr), NH₂-MIL-125, and Siogel, all with refrigerant water. Also given are details of optimal MOF (cf. Section 3.4). Heat capacities from Ehrenmann et al.^[62] (MIL-101(Cr)), Gordeeva et al.^[31] (NH₂-MIL-125), and Sapienza et al.^[46] (Siogel).

	$\Delta W [\times 10^{-4} \text{ m}^3 \text{ kg}^{-1}]$	$W_0 [\times 10^{-4} \text{ m}^3 \text{ kg}^{-1}]$	$A_{\text{infl}} [\text{kJ kg}^{-1}]$	$A_{\text{slope}} [\text{kJ kg}^{-1}]$	$c_p [\text{kJ kg}^{-1} \text{ K}^{-1}]$	$d_{\text{grain}} [\text{mm}]$	$\rho_{\text{bed}} [\text{kg m}^{-3}]$
MIL-101(Cr)	5.767	5.769	158.5	28.20	1.250	0.4	282.19
NH ₂ -MIL-125	3.164	3.194	228.7	26.78	1.045	0.4	373.85
Siogel	5.121	4.906	118.7	135.75	0.700	0.9	577.11
Optimal MOF	5.430	5.500	283.40	10.00	1.250	0.4	577.11

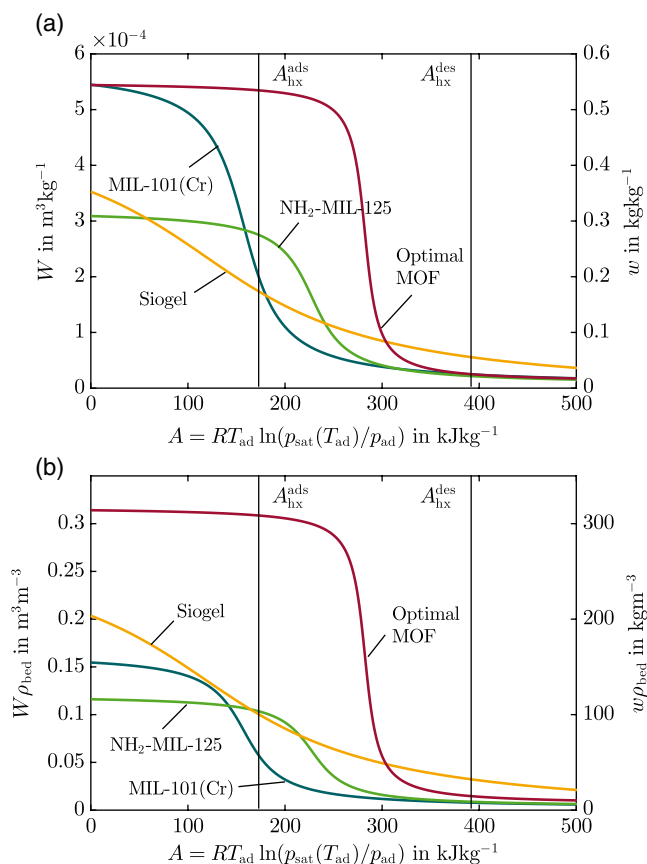


Figure 4. a) Characteristic curves $W(A)$ over adsorption potential A (Equation (1) and Equation (2)) and b) volumetric characteristic curves $W(A)\rho_{\text{bed}}$ of the investigated materials MIL-101(Cr), $\text{NH}_2\text{-MIL-125}$, Siogel, and optimal MOF (cf. Section 3.4) with refrigerant water. For a better interpretation, we multiplied the characteristic curve with the constant density of water $\rho_{\text{ad}} = 1000 \text{ kg m}^{-3}$ to receive the loading w (cf. Equation (1)) (right axis in (a) and (b)). The adsorption potentials $A_{\text{hx}}^{\text{ads}}(T_{\text{ads}}, p_{\text{evap}})$ and $A_{\text{hx}}^{\text{des}}(T_{\text{des}}, p_{\text{cond}})$ are the maximum achievable adsorption potentials during the sorption process, indicating the maximum achievable change in loading Δw (cf. Table 3).

transformed to a change in loading Δw (cf. Equation (1)), which describes the maximum change in loading Δw for the given temperature set.

Table 3 shows the change in loading for the investigated working pairs. For the typical temperature set 10/30/80 °C of an adsorption chiller, $\text{NH}_2\text{-MIL-125}$ has the highest change in loading Δw , followed by MIL-101(Cr) and Siogel. Even though MIL-

101(Cr) has the highest maximum loading and is for this reason broadly discussed in literature, it does not have the highest change in loading for the given adsorption chiller application. The reason for this change in order is the position of the inflection point of the characteristic curve A_{infl} (cf. Section 2.1). Shifting the inflection point to higher adsorption potentials (equivalent to a shift of the isotherms to lower relative pressures, cf. Equation (2)) would increase the change in loading, as discussed in Section 3.4.

In addition, the bed density ρ_{bed} is halved for the MOFs $\text{NH}_2\text{-MIL-125}$ and MIL-101(Cr) compared with Siogel. Thus, less mass of the adsorbent fits into the fixed volume of the adsorber (cf. Section 2.3), leading to less water to be adsorbed. The effect can clearly be seen when multiplying the loading with bed density $w\rho_{\text{bed}}$, resulting in the volumetric change in loading, see Figure 4b and Table 3: The volumetric change in loading $\Delta w\rho_{\text{bed}}$ for MIL-101(Cr) is 28% smaller than for Siogel.

The ranking of the adsorbents differs for other temperatures. To show this effect, we changed the condensation and adsorption temperature to 20 °C (resulting temperature set was 10/20/80 °C). A smaller condensation and adsorption temperature is beneficial for all adsorption chiller processes,^[41] since the adsorption potential at the end of adsorption $A_{\text{hx}}^{\text{ads}}(T_{\text{ads}}, p_{\text{evap}})$ decreases and the adsorption potential at the end of desorption $A_{\text{hx}}^{\text{des}}(T_{\text{des}}, p_{\text{cond}})$ increases (cf. Equation (2)), leading to a higher change in loading. In practice, the condensation and adsorption temperature is limited to the ambient temperature plus a temperature difference in the heat exchanger. Thus, temperatures below 30 °C for condensation and adsorption are generally difficult to achieve. Still, if we consider the temperature set 10/20/80 °C, MIL-101(Cr) would yield both the highest change in loading Δw and volumetric change in loading $\Delta w\rho_{\text{bed}}$ (Table 3), since the inflection point A_{infl} of MIL-101(Cr) occurs at lower adsorption potentials. However, the volumetric loading is only slightly smaller for Siogel.

In general, a higher desorption temperature leads to a higher change in loading.^[41] However, the effect of a high desorption temperature is small for the MOFs MIL-101(Cr) and $\text{NH}_2\text{-MIL-125}$: Increasing the desorption temperature increases the change in loading only slightly, because the characteristic curve's inflection point of both MOFs is closer to lower adsorption potentials (cf. Figure 4a).

Since the characteristic curve's inflection point of both MOFs is closer to lower adsorption potentials, they seem to allow lower desorption temperatures from energy sources with lower temperatures. For a desorption temperature of 60 °C, both MOFs reach a change in loading Δw almost three times higher than

Table 3. Maximum change in equilibrium loading Δw and change in volumetric loading $\Delta w\rho_{\text{bed}}$ of MIL-101(Cr), $\text{NH}_2\text{-MIL-125}$, Siogel, and the optimal MOF for the temperature sets 10/30/80, 10/20/80, and 10/30/60 °C.

	10/30/80 [°C]		10/20/80 [°C]		10/30/60 [°C]	
	Δw [g g^{-1}]	$\Delta w\rho_{\text{bed}}$ [kg m^{-3}]	Δw [g g^{-1}]	$\Delta w\rho_{\text{bed}}$ [kg m^{-3}]	Δw [g g^{-1}]	$\Delta w\rho_{\text{bed}}$ [kg m^{-3}]
MIL-101(Cr)	0.176	49.7	0.492	138.7	0.136	38.3
$\text{NH}_2\text{-MIL-125}$	0.254	94.9	0.287	107.3	0.147	54.9
Siogel	0.119	68.9	0.237	136.6	0.056	32.3
Optimal MOF	0.510	294.3	0.525	303.2	0.028	16.1

Siogel. Yet, the volumetric change in loading $\Delta w \rho_{\text{bed}}$ for $\text{NH}_2\text{-MIL-125}$ is only 1.5 times higher than for Siogel and for MIL-101(Cr) even almost identical (cf. Table 3).

In summary, MIL-101(Cr) has the highest maximum loading, but the isotherms are poorly positioned for an adsorption chiller application. For the adsorption chiller application, the change in loading is highest for $\text{NH}_2\text{-MIL-125}$. However, both MOFs MIL-101(Cr) and $\text{NH}_2\text{-MIL-125}$ have low densities ρ_{bed} compared with Siogel, reducing the effect of high changes in loading Δw . As a first design rule, we can conclude that equilibrium properties of MOFs need to fit the process temperatures in order to achieve a high change in loading. Besides, a high density is important for a high volumetric change in loading.

3.2. Heat and Mass Transfer Coefficients

The discussed change in loading corresponds to equilibrium conditions: In actual adsorption chillers, heat transfer and diffusion resistances slow down the sorption process. Heat transfer and diffusion coefficients need to be identified to comprehensively evaluate the performance of MOFs for thermal energy conversion. To determine the heat transfer and diffusion coefficients, we perform IR-LTJ experiments and use a dynamic model (cf. Section 2.2). For the model, the following information is necessary: The equilibrium properties, the mean grain size d_{grain} , the packed bed density ρ_{bed} , and the heat capacity c_p , summarized in Table 2.

Table 4 shows the resulting effective heat transfer and diffusion coefficients U_{eff} and D_{eff} of the investigated materials. The experimental data can be found Section C, Supporting Information. The effective heat transfer coefficient U_{eff} during adsorption and desorption is almost half for $\text{NH}_2\text{-MIL-125}$ and MIL-101(Cr) compared with Siogel. The lower packed-bed density of the MOFs (cf. Table 2) might lead to thermal insulation and thus lower heat transfer coefficients. To our knowledge, no heat transfer coefficients for the studied MOFs are reported. Only one value for thermal conductivity is reported for MOF-5 with $0.32 \text{ W m}^{-1} \text{ K}^{-1}$.^[63] The value is also almost half of thermal conductivity as for silica gel with $0.55 \text{ W m}^{-1} \text{ K}^{-1}$.^[64] Thus, our findings are in line with the literature.

Also, the effective diffusion coefficient D_{eff} is considerably lower for the MOFs: It is lower by a factor of 20–40 compared with Siogel. The mean pore size of $\text{NH}_2\text{-MIL-125}$ is 5.9 \AA ^[31] and thus smaller than for Siogel with 20 \AA ,^[46] probably leading

Table 4. Effective heat transfer coefficients U_{eff} and effective diffusion coefficients D_{eff} for adsorption and desorption of the investigated MOFs MIL-101(Cr) and $\text{NH}_2\text{-MIL-125}$ and the benchmark Siogel, all with the refrigerant water. The coefficients are determined by the IR-LTJ method^[36] for a packed-bed configuration with 1 mm layer height and a temperature set $10/30/80^\circ\text{C}$. The experimental data can be found Section C, Supporting Information. Coefficients for Siogel taken from Graf et al.^[36]

	$U_{\text{eff}}^{\text{ads}} [\text{W m}^{-2} \text{ K}^{-1}]$	$D_{\text{eff}}^{\text{ads}} [\text{m}^2 \text{ s}^{-1}]$	$U_{\text{eff}}^{\text{des}} [\text{W m}^{-2} \text{ K}^{-1}]$	$D_{\text{eff}}^{\text{des}} [\text{m}^2 \text{ s}^{-1}]$
MIL-101(Cr)	111.0	6.22×10^{-11}	114.7	3.09×10^{-10}
$\text{NH}_2\text{-MIL-125}$	164.0	9.79×10^{-11}	165.3	1.51×10^{-10}
Siogel	223.6	1.48×10^{-9}	277.4	9.89×10^{-9}

to smaller effective diffusion coefficients. On the contrary, however, MIL-101(Cr) has considerably larger pores with pore sizes between 24 and 36 \AA compared with Siogel.^[10,13] To our knowledge, diffusion coefficients for MIL-101(Cr) with water have not been reported. Yet, the diffusion process has been discussed for MIL-101(Cr) with other adsorptives than water: Ma et al.^[65] found that at early stages of the adsorption process, the diffusion rate of the working pair MIL-101/isobutane is considerably lower than for activated carbon/isobutane. For the working pair MIL-101(Cr)/ethanol, Saha et al.^[66] determined a higher activation energy, leading to slower adsorption rates, compared with activated carbon/ethanol. Also, Rezk et al.^[67] noted that the adsorption kinetics of the working pair silica gel/water are faster than for MIL-100/water. For the working pair silica gel/water, Gurgel et al.^[64] determined an effective diffusion coefficient during adsorption of $1.9 \times 10^{-9} \text{ m}^2 \text{ s}^{-1}$, which is in line with our findings. This literature review supports our finding that the diffusion in MIL-101(Cr) is slower than for commonly used adsorbents regardless of the adsorptive.

Low heat transfer and diffusion coefficients inhibit the sorption process, and thus reduce the power density, which we discuss in the next section. As a second design rule, we conclude that the heat transfer coefficients of MOFs need to be increased by factor 2 and diffusion coefficients by one magnitude compared with Siogel

3.3. Performance of MOFs in Adsorption Chillers

The previously discussed equilibrium properties and heat transfer and diffusion coefficients are the necessary inputs for a dynamic model of an adsorption chiller. The model allows us to determine the efficiency and power density of the MOFs in terms of COP and VCP, respectively (cf. Section 2.3). Figure 5 shows the Pareto frontier of power density VCP over efficiency COP for the reference case $10/30/80^\circ\text{C}$ as well as for the varied temperature sets.

For the standard temperature set ($10/30/80^\circ\text{C}$), even though MIL-101(Cr) has the maximum adsorption capacity

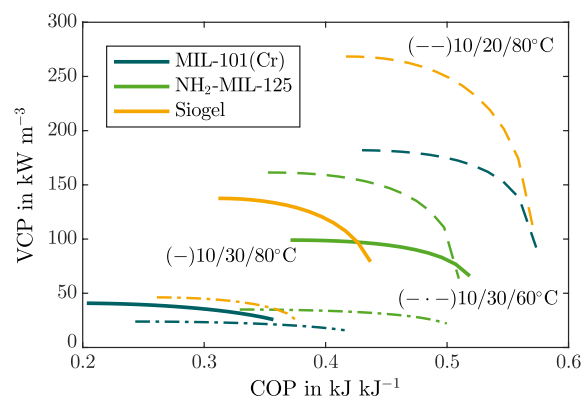


Figure 5. Pareto frontiers of power density VCP (cf. Equation (5)) over efficiency COP (cf. Equation (4)) for the adsorbents MIL-101(Cr) (in blue), $\text{NH}_2\text{-MIL-125}$ (in green), and Siogel (in yellow). Pareto frontiers for the reference case $10/30/80^\circ\text{C}$ (solid lines) and in addition $10/20/80^\circ\text{C}$ (dashed lines) and $10/30/60^\circ\text{C}$ (dash-dotted lines). For a colored figure, the reader is referred to the web version of this article.

(cf. Section 3.1), both Siogel and $\text{NH}_2\text{-MIL-125}$ outperform MIL-101(Cr) regarding both efficiency COP and power density VCP: The maximum efficiency of MIL-101(Cr) is 0.36 and thus 19% smaller than for Siogel (0.43) and 44% smaller than for $\text{NH}_2\text{-MIL-125}$ (0.52). As discussed in Section 3.1, the reason is the inflection point of MIL-101(Cr)'s equilibrium properties. In addition, we keep the adsorbent volume constant (cf. Section 2.3). Since the bed density ρ_{bed} is lower for the MOFs compared with Siogel (cf. Table 2), the mass of MOFs in the constant volume of the adsorber is lower as well, leading to a lower change in loading multiplied with the bed density $\Delta w \rho_{\text{bed}}$ for MIL-101(Cr) than for Siogel and $\text{NH}_2\text{-MIL-125}$ (cf. Table 3).

It is noteworthy that the maximum power density VCP is not achieved by any MOF but by Siogel: Siogel reaches a maximum power density of 137.6 kW m^{-3} , whereas for $\text{NH}_2\text{-MIL-125}$ the maximum power density is 99.1 kW m^{-3} and thus 28% smaller, and for MIL-101(Cr) the maximum power density is 40.8 kW m^{-3} and thus even 70% smaller than for Siogel. Since Siogel has higher heat transfer and diffusion coefficients than the MOFs (cf. Table 4), the power density is higher. To conclude, Siogel and $\text{NH}_2\text{-MIL-125}$ outperform MIL-101(Cr) regarding efficiency and power density. For high power densities, Siogel is preferable, whereas for high efficiencies $\text{NH}_2\text{-MIL-125}$ is preferable for the reference case.

When reducing the recooling temperature from 30 to 20 °C, all materials perform better, as the change in loading increases, as discussed in Section 3.1. For this case (10/20/80 °C), MIL-101(Cr) has a maximum efficiency COP of 0.57 and a maximum power density VCP of 182.0 kW m^{-3} and thereby outperforms $\text{NH}_2\text{-MIL-125}$ with a maximum efficiency of 0.51 and a maximum power density of 161.4 kW m^{-3} . This change in order shows the high sensitivity of performance on the temperatures in the application. However, Siogel still outperforms MIL-101(Cr) with an equally high maximum efficiency of 0.57 and a 32% higher maximum power density of 268.4 kW m^{-3} . Again, Siogel's high heat transfer and diffusion coefficients and high density compared with MIL-101(Cr) overcompensate the smaller change in loading.

From the equilibrium properties, it can be seen that a high desorption temperature is not necessary for MOFs to achieve a high change in loading (cf. Section 3.1). To show where this property could be beneficial, we decreased the desorption temperature from 80 to 60 °C. Then, the change in loading for MIL-101(Cr) decreases by only 22%, whereas for $\text{NH}_2\text{-MIL-125}$ by 44% and for Siogel by 53% (cf. Table 3). The maximum efficiency of MIL-101(Cr) even increases compared with the reference case 10/30/80 °C because the high desorption temperature is not necessary for a high change in loading but increases the amount of heat that needs to be recooled, leading to a smaller efficiency. Still, the change in loading for $\text{NH}_2\text{-MIL-125}$ is higher than for MIL-101(Cr), resulting in a 19% higher maximum efficiency COP of 0.50 compared with 0.42. Additionally, $\text{NH}_2\text{-MIL-125}$ has a higher maximum power density VCP of 35.0 kW m^{-3} compared with 23.9 kW m^{-3} for MIL-101(Cr). Therefore, $\text{NH}_2\text{-MIL-125}$ still outperforms MIL-101(Cr). For Siogel, the maximum power density is 46.2 kW m^{-3} and thus slightly higher than for $\text{NH}_2\text{-MIL-125}$. However, the power density decreases for all materials considerably, as the lower

desorption temperature reduces the driving force for heat transfer. As for the reference case, for high power densities, Siogel is preferable; for high efficiencies, $\text{NH}_2\text{-MIL-125}$ is preferable.

In summary, Siogel is the best choice, when high power densities are desired, whereas $\text{NH}_2\text{-MIL-125}$ is in most cases beneficial for high efficiencies. Currently, $\text{NH}_2\text{-MIL-125}$ is not competitive in the perspective of high power densities, compared with the commercial adsorbent Siogel, whereas MIL-101(Cr) is not competitive at all, despite its high maximum loading. In the next section, we quantify the potential of MOFs for use in adsorption chillers and derive how the performance of MOFs regarding efficiency and power density can be improved by applying our proposed design rules (see Section 3.1 and Section 3.2).

3.4. The Potential of MOFs

In this section, we discuss how an optimal MOF could perform in an adsorption chiller. For the optimal MOF, obviously, the change in loading and density should be as high as possible for high efficiencies; heat transfer and diffusion should be as fast as possible for high power densities. To limit the study to realistic values, we define an optimal MOF by combining the most favorable properties of all studied materials, i.e., the adsorption capacity is equal to the maximum adsorption capacity of MIL-101(Cr) and the density, heat transfer, and diffusion coefficients are equal to the properties of Siogel, Table 2.

As discussed in Section 3.1, the position of the characteristic curve has a high influence on the actual change in loading in the application.^[68] For this reason, Erdős et al.^[21] screened several MOFs regarding their adsorption capacity for a fixed application. Also, Boman et al.^[69] screened several adsorbent materials by considering the position of the characteristic curve. In both studies methanol and ethanol are used as refrigerants, whereas in this study, we investigate the potential of MOFs with water as the refrigerant.

In addition to these properties, the shape of the characteristic curve has a high influence on power density: Okunev et al.^[70] and Glaznev et al.^[71] found that the concave shape of the adsorption isobars influences the sorption process and leads to a slower adsorption process than the desorption process. Aristov^[72] concluded in a theoretic study that a step adsorption isobar is preferable and Okunev et al.^[73] refined this study by modeling the adsorption isobar with a consistent model for equilibrium, heat transfer, and diffusion. These authors simulated the isobaric adsorption and desorption stages for an exemplary temperature set and identified the optimal position of the step isobar. The optimal step isobar position shortened the adsorption and desorption times by a factor of 3 compared with the reference, increasing the power density also by a factor of 3.

The step isobar can be translated into the characteristic curve of the Dubinin model (cf. Figure 1): a step isobar also corresponds to a step characteristic curve, which is achieved by small values for the slope of the characteristic curve A_{slope} (cf. Equation (3)). In addition, the driving force for heat transfer ($T_{\text{ad}} - T_{\text{hx}}$) can be translated into the Dubinin model. For this purpose, we assume an exponential correlation between temperature and the corresponding saturation pressure used in the adsorption potential (Equation (2)), e.g., with the Antoine equation.^[74] Then, the

driving force for heat transfer ($T_{ad} - T_{hx}$) is proportional to the difference in adsorption potentials ($A_{ad} - A_{hx}$). In Figure 1, the benefit of the step isobar is visualized: Due to the step, the driving force ($A_{ad} - A_{hx}$) stays constant at its maximum value during the sorption process. In addition, the optimal position of the inflection point A_{infl}^{opt} can be identified as the mean of A_{hx}^{ads} and A_{hx}^{des} , if assuming identical heat transfer coefficients $U_{eff}^{ads} = U_{eff}^{des}$ for adsorption and desorption.

A step isobar is also optimal for mass transfer: The driving force for mass transfer is the difference between equilibrium loading w_{eq} and the actual loading of the adsorbent w : $[w_{eq}(p_v, T_{ad}) - w(p_{ad}, T_{ad})]$. For a steeper isobar, the equilibrium loading w_{eq} changes faster, leading to a constant and high driving force.

Thus, a step isobar, or translated into the Dubinin model, a step characteristic curve, is optimal for maximum heat and maximum mass transfer, resulting in high power densities. The resulting equilibrium properties of the optimal MOF are shown in Figure 4a and summarized in Table 2.

In addition to the optimal MOF that summarizes all the best characteristics, we study the effect of improving a single characteristic, i.e., changing the inflection point, the density, and heat transfer and diffusion coefficients to the value of Siogel.

Figure 6(1) shows the resulting Pareto frontiers for NH_2 -MIL-125 with modified characteristics. When changing the inflection point of NH_2 -MIL-125 to the optimal position, the maximum power density VCP increases by 22%, whereas the efficiency COP stays almost constant. The efficiency stays constant, because the change in loading is constant, when changing the inflection point of NH_2 -MIL-125. The largest influence on the efficiency comes from changing the density of NH_2 -MIL-125 to the density of Siogel. Then, the maximum efficiency increases by 16% (and the maximum power density by 21%). The largest influence on the power density comes from higher heat transfer and diffusion coefficients: When changing the heat transfer and diffusion coefficients of NH_2 -MIL-125 to Siogel's heat transfer and diffusion coefficients, the maximum power density increases almost by factor 2 from 99.1 to 193.3 $kW m^{-3}$.

Modifying all properties to the best values results in the optimal MOF. The maximum power density VCP is 265.1 $kW m^{-3}$ and thus 2.7 times higher than NH_2 -MIL-125's maximum power density of 99.1 $kW m^{-3}$ and still 93% higher than Siogel's maximum power density. Also, the maximum efficiency COP of the optimal MOF is 0.73 and thus 40% higher than for NH_2 -MIL-125 and 67% higher than for Siogel. Due to the higher change in loading multiplied by bed density $\Delta w \rho_{bed}$ (cf. Table 3), both the maximum power density and efficiency of the optimal MOF increase.

Figure 6(2) shows the resulting Pareto frontiers for MIL-101(Cr) with modified characteristics. The inflection point of the characteristic curve A_{infl} has the largest influence on both power density VCP and efficiency COP: Changing MIL-101(Cr)'s inflection point to the optimal inflection point leads to a 2.8 times higher maximum power density and a 67% higher maximum efficiency. By moving the inflection point, the change in loading increases, leading to both higher power densities and efficiencies. Also, the driving force for heat transfer is constant at a high level, as discussed earlier (cf. Figure 1). The modified

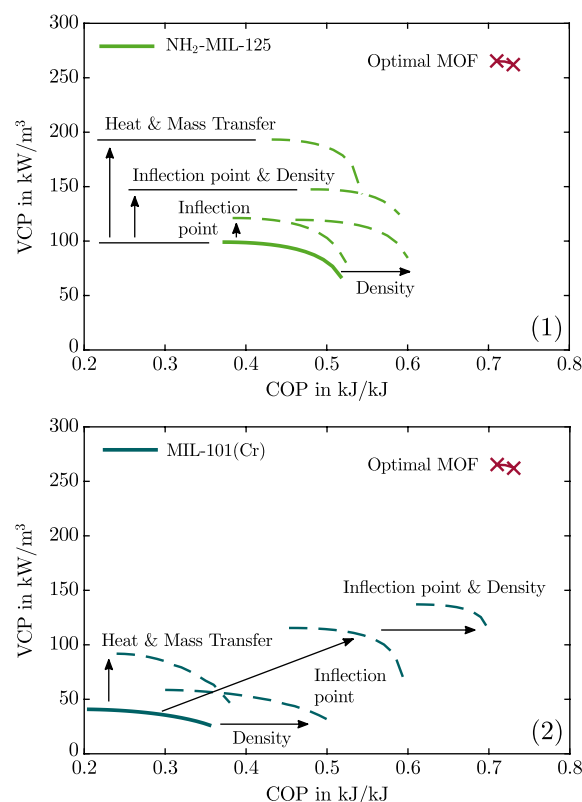


Figure 6. Pareto frontiers of power density VCP over efficiency COP for (1) NH_2 -MIL-125 (solid line) and modified NH_2 -MIL-125 (dashed lines) and (2) for MIL-101(Cr) (solid line) and modified MIL-101(Cr) (dashed lines) with Siogel properties: density, heat transfer and diffusion coefficients, or optimal position of inflection point. Also shown is the Pareto frontier of the optimal MOF (cf. Figure 4 (a)) for the reference case 10/30/80 °C. For a colored figure, the reader is referred to the web version of this article.

MIL-101(Cr) would outperform Siogel now, with almost the same power density but a considerably higher efficiency. As for modifying the density of NH_2 -MIL-125 to Siogel's density, modifying MIL-101(Cr)'s density mainly leads to an increase in maximum efficiency by 56% compared with MIL-101(Cr) with optimal position of the inflection point. Changing the heat transfer and diffusion coefficients of MIL-101(Cr) to the heat transfer and diffusion coefficients of Siogel increases the maximum power density by a factor of 2.3.

We find that the choice of adsorbent material has a greater influence than the choice of adsorber design: In a study of Bau et al.,^[37] the influence of adsorber geometry is broadly investigated with a similar approach as in this study. The authors found that from optimizing the number of fins of the adsorber, COP could be increased by 12% and the SCP could be almost doubled. In our study, we found that both COP and power density VCP could almost be doubled when the optimal adsorbent material is used. Thus, especially when it comes to high COP values, the choice of adsorbent material seems to be more crucial than the choice of adsorber geometry. Still, optimizing both adsorbent material and geometry is required to explore the full potential.

In conclusion, to increase both the power density and efficiency of MOFs, the highest potential for improvement comes from the position of the inflection point of the equilibrium properties. Therefore and as the first design rule when designing MOFs, great attention should be directed to fitting the equilibrium properties to the process temperatures. As the second design rule, increasing the heat transfer and diffusion coefficients is necessary to increase the power density. Besides, increasing the density leads to higher efficiencies.

These generic guidelines toward an optimal MOF should be helpful to guide material development or identification. While the derivation of specific synthesis strategies is beyond our own scope of work, we hope that the derived guidelines help material developers properly assess novel materials.

4. Conclusions

MOFs are highly promising materials: High water uptake capacities suggest that MOFs are well suited for sustainable thermal energy conversion, such as for the adsorption chillers discussed here. However, most attention is currently often given to maximize adsorption capacity.

The MOFs MIL-101(Cr) and NH₂-MIL-125 offer a high adsorption capacity for water and have therefore been suggested for sustainable thermal energy conversion in adsorption heat pumps and chillers. In this study, we showed that these MOFs are still only partly competitive to commercial silica gels.

For this purpose, we combined small-scale experiments with dynamic modeling of full-scale adsorption chillers: First, we determined heat transfer and diffusion coefficients with the small-scale IR-LTJ method. To our knowledge, we provided the first data on heat transfer and diffusion coefficients for the MOFs NH₂-MIL-125 and MIL-101(Cr). Second, we used the adsorbent information in a dynamic model of a full-scale adsorption chiller to determine the COP as a measure for the system's efficiency and the VCP as a measure for the power density and system size.

For the practically relevant temperature set 10/30/80 °C, we found that NH₂-MIL-125 reduces the power density by 28% compared with the benchmark Siogel. However, NH₂-MIL-125 increases the efficiency by 18% compared with Siogel. Noteworthy, MIL-101(Cr) is not suitable at all for the temperature set 10/30/80 °C, despite being the adsorbent with the highest adsorption capacity. The same results apply for lower temperatures for desorption, adsorption, and condensation. For lower adsorption and condensation temperatures, both MOFs are clearly outperformed by Siogel.

Analysis of the model allows to derive design rules to exploit the full potential of MOFs for adsorption chillers. Material development of MOFs should focus on three design rules: 1) Matching the shape and position of the isotherms to the given application: Since the possibilities to tune the structure of MOFs are countless, the shape of the equilibrium isotherms should be step wise and tailored to the specific temperature conditions. Moving the step position of current MOFs would give power densities in the same range as for the commercial adsorbent Siogel but with 1.5 times higher efficiencies. 2) Increasing heat transfer coefficients by factor 2 and diffusion coefficients by 1–2 orders of

magnitude. Then, the power density would increase by a factor of more than 2. 3) Increasing the density by factor 2 to increase the efficiency by factor 1.5.

Applying all three design rules of material development would lead to an optimal MOF allowing for a maximum power density of 350.5 kW m⁻³ and efficiency of 0.73, both values being almost twice as high for Siogel—with the same adsorption capacity already achieved by MOFs today. Such optimal MOFs would be able to realize their promise to serve for more sustainable energy conversion in adsorption chillers.

In this study, we investigated the MOFs MIL-101(Cr) and NH₂-MIL-125 with water as the adsorptive. While we believe that the presented methodology extends to other MOFs or other adsorptives (e.g., methanol and ethanol), quantitative results will differ and require further study.

Supporting Information

Supporting Information is available from the Wiley Online Library or from the author.

Acknowledgements

This work was conducted within the project “TailorSorb – Tailored adsorbents for stationary adsorption thermal energy transformation” (03SF0515A). The project was funded by the German Federal Ministry of Education and Research (BMBF) within the funding priority “Materialforschung für die Energiewende.”

Conflict of Interest

The authors declare no conflict of interest.

Keywords

dynamic modeling, infrared large temperature jump, metal–organic frameworks, refrigerant water

Received: May 26, 2019

Revised: July 28, 2019

Published online:

- [1] H. Furukawa, K. E. Cordova, M. O’Keeffe, O. M. Yaghi, *Science* **2013**, 341, 1230444.
- [2] C. Jürgen, *Chem. Ing. Tech.* **2018**, 90, 1759.
- [3] L. Zhu, X.-Q. Liu, H.-L. Jiang, L.-B. Sun, *Chem. Rev.* **2017**, 117, 8129.
- [4] N. A. Qasem, R. Ben-Mansour, M. A. Habib, *Appl. Energy* **2018**, 210, 317.
- [5] J. M. Simmons, H. Wu, W. Zhou, T. Yildirim, *Energy Environ. Sci.* **2011**, 4, 2177.
- [6] Z. Zhang, Z.-Z. Yao, S. Xiang, B. Chen, *Energy Environ. Sci.* **2014**, 7, 2868.
- [7] S. Keskin, D. S. Sholl, *Energy Environ. Sci.* **2010**, 3, 343.
- [8] M. Beckner, A. Dailly, *Appl. Energy* **2016**, 162, 506.
- [9] J. A. Mason, J. Oktawiec, M. K. Taylor, M. R. Hudson, J. Rodriguez, J. E. Bachman, M. I. Gonzalez, A. Cervellino, A. Guagliardi, C. M. Brown, P. L. Llewellyn, N. Masciocchi, J. R. Long, *Nature*, **2015**, 527, 357.

- [10] S. Kayal, B. Sun, A. Chakraborty, *Energy*, **2015**, 91, 772.
- [11] M. Bastos-Neto, C. Patzschke, M. Lange, J. Mollmer, A. Moller, S. Fichtner, C. Schrage, D. Lassig, J. Lincke, R. Staudt, H. Krautscheid, R. Glaser, *Energy Environ. Sci.* **2012**, 5, 9269.
- [12] A. Morozan, F. Jaouen, *Energy Environ. Sci.* **2012**, 5, 9269.
- [13] J. Canivet, A. Fateeva, Y. Guo, B. Coasne, D. Farrusseng, *Chem. Soc. Rev.* **2014**, 43, 5594.
- [14] H. Kim, S. Yang, S. R. Rao, S. Narayanan, E. A. Kapustin, H. Furukawa, A. S. Umans, O. M. Yaghi, E. N. Wang, *Science* **2017**, 356, 430.
- [15] A. J. Rieth, S. Yang, E. N. Wang, M. Dincă, *ACS Central Sci.* **2017**, 3, 668.
- [16] A. Elsayed, E. Elsayed, R. AL-Dadah, S. Mahmoud, A. Elshaer, W. Kaialy, *Appl. Energy* **2017**, 186, 509.
- [17] M. F. de Lange, K. J. Verouden, T. J. Vlugt, J. Gascon, F. Kapteijn, *Chem. Rev.* **2015**, 115, 12205.
- [18] B. Choudhury, B. B. Saha, P. K. Chatterjee, J. P. Sarkar, *Appl. Energy* **2013**, 104, 554.
- [19] F. Meunier, *Appl. Therm. Eng.* **2013**, 61, 830.
- [20] M. F. de Lange, B. L. van Velzen, C. P. Ottevanger, K. J. F. M. Verouden, L.-C. Lin, T. J. H. Vlugt, J. Gascon, F. Kapteijn, *Langmuir* **2015**, 31, 12783.
- [21] M. Erdős, M. F. de Lange, F. Kapteijn, O. A. Moulton, T. J. H. Vlugt, *ACS Appl. Mater. Interfaces* **2018**, 10, 27074.
- [22] A. Rezk, R. AL-Dadah, S. Mahmoud, A. Elsayed, *Appl. Energy* **2013**, 112, 1025.
- [23] H. Kummer, M. Baumgartner, P. Hügenell, D. Fröhlich, S. K. Henninger, R. Gläser, *Appl. Therm. Eng.* **2017**, 117, 689.
- [24] F. Jeremias, D. Fröhlich, C. Janiak, S. K. Henninger, *New J. Chem.* **2014**, 38, 1846.
- [25] M. Solovyeva, L. Gordeeva, T. Krieger, Y. Aristov, *Energy Conver. Manage.* **2018**, 174, 356.
- [26] J. J. Jenks, R. K. Motkuri, W. TeGrotenhuis, B. K. Paul, B. P. McGrail, *Heat Transfer Eng.* **2017**, 38, 1305.
- [27] Y. I. Aristov, *Appl. Therm. Eng.* **2012**, 42, 18.
- [28] Y. I. Aristov, *Renewable Energy*, **2017**, 110, 105.
- [29] A. Sharafian, M. Bahrami, *Renewable Sustainable Energy Rev.* **2014**, 30, 440.
- [30] S. J. Metcalf, R. E. Critoph, Z. Tamainot-Telto, *Int. J. Refrig.* **2012**, 35, 571.
- [31] L. G. Gordeeva, M. V. Solovyeva, Y. I. Aristov, *Energy* **2016**, 100, 18.
- [32] D. Lenzen, P. Bendix, H. Reinsch, D. Fröhlich, H. Kummer, M. Möllers, P. P. C. Hügenell, R. Gläser, S. Henninger, N. Stock, *Adv. Mater.* **2018**, 30, 1705869.
- [33] M. Rubio-Martinez, C. Avci-Camur, A. W. Thornton, I. Imaz, D. Maspocho, M. R. Hill, *Chem. Soc. Rev.* **2017**, 46, 3453.
- [34] M. Sánchez-Sánchez, N. Getachew, K. Díaz, M. Díaz-García, Y. Chebude, I. Díaz, *Green Chem.* **2015**, 17, 1500.
- [35] Y. Seo, J. Yoon, J. Lee, U. Lee, Y. Hwang, C.-H. Jun, P. Horcajada, C. Serre, J. Chang, *Microporous and Mesoporous Mater.* **2012**, 157, 137.
- [36] S. Graf, F. Lanzerath, A. Bardow, *Appl. Therm. Eng.* **2017**, 126, 630.
- [37] U. Bau, P. Hoseinpoori, S. Graf, H. Schreiber, F. Lanzerath, C. Kirches, A. Bardow, *Appl. Therm. Eng.* **2017**, 125, 1565.
- [38] G. Férey, C. Mellot-Draznieks, C. Serre, F. Millange, J. Dutour, S. Surblé, I. Margiolaki, *Science* **2005**, 309, 2040.
- [39] A. Khutia, H. U. Rammelberg, T. Schmidt, S. Henninger, C. Janiak, *Chem. Mater.* **2013**, 25, 790.
- [40] F. Jeremias, V. Lozan, S. K. Henninger, C. Janiak, *Dalton Trans.* **2013**, 42, 15967.
- [41] Y. Aristov, *Appl. Therm. Eng.* **2014**, 72, 166.
- [42] Z. S. Lu, R. Z. Wang, Z. Z. Xia, Q. B. Wu, Y. M. Sun, Z. Y. Chen, *Appl. Therm. Eng.* **2011**, 31, 3636.
- [43] B. B. Saha, S. Koyama, J. B. Lee, K. Kuwahara, K. Alam, Y. Hamamoto, A. Akisawa, T. Kashiwagi, *Int. J. Multiphase Flow* **2003**, 29, 1249.
- [44] K. Leus, T. Bogaerts, J. D. Decker, H. Depauw, K. Hendrickx, H. Vrielinck, V. V. Speybroeck, P. V. D. Voort, *Microporous Mesoporous Mater.* **2016**, 226, 110.
- [45] S.-I. Kim, T.-U. Yoon, M.-B. Kim, S.-J. Lee, Y. K. Hwang, J.-S. Chang, H.-J. Kim, H.-N. Lee, U.-H. Lee, Y.-S. Bae, *Chem. Eng. J.* **2016**, 286, 467.
- [46] A. Sapienza, A. Velte, I. Gernik, A. Frazzica, G. Földner, L. Schnabel, Y. Aristov, *Renewable Energy*, **2017**, 110, 40.
- [47] M. M. Dubinin, *J. Colloid Interface Sci.* **1967**, 23, 487.
- [48] D. Schawe, *PhD Thesis*, Universität Stuttgart, **2001**.
- [49] M. F. de Lange, *PhD Thesis*, Technische Universiteit Delft, **2015**.
- [50] S. Graf, F. Lanzerath, A. Sapienza, A. Frazzica, A. Freni, A. Bardow, *Appl. Therm. Eng.* **2016**, 98, 900.
- [51] F. Lanzerath, U. Bau, J. Seiler, A. Bardow, *Sci. Technol. Built Environ.* **2015**, 21, 248.
- [52] A. Sharafian, S. M. N. Mehr, P. C. Thimmaiah, W. Huttema, M. Bahrami, *Energy* **2016**, 112, 481.
- [53] U. Bau, F. Lanzerath, M. Gräber, S. Graf, H. Schreiber, N. Thielen, A. Bardow, in *Proc. of the 10th Int Modelica Conf.*, Linköping University, Linköping, **2014**, pp. 875–883.
- [54] P. A. Fritzson, *Principles of Object-Oriented Modeling and Simulation with Modelica 2.1*, IEEE Press and Wiley-Interscience, Piscataway, NJ and New York **2004**.
- [55] E. Glueckauf, *Trans. Faraday Soc.* **1955**, 51, 1540.
- [56] M. Gräber, K. Kosowski, C. Richter, W. Tegethoff, *Math. Comput. Modell. Dyn. Syst.* **2010**, 16, 195.
- [57] E. W. Lemmon, M. L. Huber, M. O. McLinden, N. I. S. T. *Standard Reference Database 23: Reference Fluid Thermodynamic and Transport Properties-REFPROP, Version 9.1*, National Institute of Standards and Technology, Gaithersburg, MD **2013**.
- [58] J. D. Cox, D. D. Wagman, V. A. Medvedev, *CODATA Key Values for Thermodynamics*, Hemisphere Publishing Corp., New York **1989**.
- [59] M. W. Chase, *NIST-JANAF Thermochemical Tables, Journal of Physical and Chemical Reference Data Monographs or Supplements*, 4th ed., American Institute of Physics, College Park, MD **1998**.
- [60] D. B. Leineweber, I. Bauer, H. G. Bock, J. P. Schlöder, *Comput. Chem. Eng.* **2003**, 27, 157.
- [61] S. Graf, *PhD Thesis*, RWTH Aachen University, **2018**.
- [62] J. Ehrenmann, S. K. Henninger, C. Janiak, *Eur. J. Inorg. Chem.* **2011**, 2011, 471.
- [63] B. Huang, Z. Ni, A. Millward, A. McGaughey, C. Uher, M. Kaviany, O. Yaghi, *Int. J. Heat Mass Transfer*, **2007**, 50, 405.
- [64] J. Gurgel, L. A. Filho, P. Grenier, F. Meunier, *Adsorption*, **2001**, 7, 211.
- [65] L. Ma, H. Yang, Q. Wu, Y. Yin, Z. Liu, Q. Cui, H. Wang, *Energy*, **2015**, 93, 786.
- [66] B. B. Saha, I. I. El-Sharkawy, T. Miyazaki, S. Koyama, S. K. Henninger, A. Herbst, C. Janiak, *Energy*, **2015**, 79, 363.
- [67] A. Rezk, R. AL-Dadah, S. Mahmoud, A. Elsayed, *Int. J. Heat Mass Transfer* **2012**, 55, 7366.
- [68] M. H. Bagheri, S. N. Schiffrés, *Langmuir*, **2018**, 34, 1908.
- [69] D. B. Boman, D. C. Hoysall, D. G. Pahinkar, M. J. Ponkala, S. Garimella, *Appl. Therm. Eng.* **2017**, 123, 422.
- [70] B. N. Okunev, A. P. Gromov, L. I. Heifets, Y. I. Aristov, *Int. J. Heat Mass Transfer*, **2008**, 51, 246.
- [71] I. S. Glaznev, D. S. Ovoshchnikov, Y. I. Aristov, *Int. J. Heat Mass Transfer*, **2009**, 52, 1774.
- [72] Y. I. Aristov, *Int. J. Refrig.* **2009**, 32, 675.
- [73] B. N. Okunev, A. P. Gromov, Y. I. Aristov, *Appl. Therm. Eng.* **2013**, 53, 89.
- [74] P. Stephan, K. Schaber, K. Stephan, F. Mayinger, *Thermodynamik*, 19th ed, Springer, Berlin **2013**.